

38. SEISMIC PROPERTIES OF FLOOD BASALTS FROM HOLE 917A DOWNHOLE DATA, SOUTHEAST GREENLAND VOLCANIC MARGIN¹

Sverre Planke² and Herve Cambray³

ABSTRACT

Ocean Drilling Program Hole 917A penetrated 779 m of subaerially emplaced basalts and dacites near the landward edge of the seaward-dipping reflector sequences on the southeast Greenland volcanic margin. Wireline logs were recorded in a 430-m interval covering four very thin sediment units and 48 lava units with mean and maximum thickness of 8.9 m and 53 m, respectively. Seismic compressional-, shear-, and tube-wave velocities were obtained by slowness-time coherency inversion of sonic waveform data. The compressional-wave velocity log shows asymmetric cyclic variations, with velocities of 2.5 to 5.5 km/s in the brecciated and vesicular flow tops, and high velocities, 5 to 6 km/s, in the massive and fractured central and lower part of the lavas. The variations in velocity are attributed to systematic changes in total porosity, pore geometry, and alteration. The shear-wave velocity log recorded in high-velocity ($V_s > 1.5$ km/s) intervals correlate well with the compressional-wave velocity log. High shear-wave amplitudes identified near numerous high-impedance boundaries are related to mode-conversion within the lava pile. V_p/V_s ratios of 1.8 to 2.0 are recorded throughout the sequence, with no systematic variations. The normalized tube-wave energy log is broadly inversely proportional to the velocity logs, with low energy values in fractured massive intervals and high energy values near unit boundaries and within the top part of the lavas. Comparison of conventional logs and the Formation MicroScanner image gives high confidence to the usefulness of conventional logs in terms of recording downhole textural and lithologic variations in flood basalt terrains. The average velocity in the lava pile is 4.17 km/s, corresponding to 4.05 km/s obtained from the interpretation of seismic reflection data, and is primarily a function of the average lava unit thickness.

INTRODUCTION

The main target of Ocean Drilling Program (ODP) Leg 152 was to sample breakup volcanics on the southeast Greenland Margin to study the influence of the Iceland mantle plume on the early Cenozoic continental breakup and seafloor spreading (Larsen, Saunders, Clift, et al., 1994). The leg was successful, as volcanics were recovered from four drill holes along the EG63-transect (Figs. 1, 2). These four holes penetrated the upper part of the seaward-dipping reflector sequences (SDRS) imaged on seismic reflection data. The entire volcanic succession at Site 917 was drilled, and a 779-m-thick sequence of subaerially emplaced lava flows was found.

Evidence of excessive volcanism during the continental breakup is found on passive rifted margins worldwide, primarily based on the interpretation of SDRS on seismic reflection data (Coffin and Eldholm, 1994; Eldholm et al., 1995). Voluminous volcanic sequences have been mapped along the northeast Atlantic margins on seismic reflection data over the past two decades (Fig. 1), where up to 6-km-thick SDRS are found along the conjugate margins (e.g., Hinz et al., 1987; White et al., 1987; Larsen, 1990). Drilling of the landward parts (feather-edges) of the SDRS has confirmed that they consist of subaerially emplaced flood basalts (Roberts, Schnikter, et al., 1984; Eldholm, Thiede, Taylor, et al., 1987; Larsen, Saunders, Clift, et al., 1994).

Seismic data provide the best image of the extent and volume of breakup-related volcanics along the submerged parts of volcanic margins. However, good quality vertical incidence (reflection) seismic data are often difficult to obtain in areas affected by volcanism (e.g., Boldreel et al., 1994; Blystad et al., 1995). The crustal structure of volcanic margins is thus commonly interpreted from lower-resolu-

tion wide-angle seismic data (e.g., Zehnder et al., 1990). Studies of physical properties of breakup volcanics may lead to improved understanding of seismic wave propagation in these volcanic sequences, which, in turn, may lead to improved vertical incidence seismic images.

The comprehensive suite of downhole logs recorded in Hole 917A provides a unique possibility to study the seismic properties of flood basalts. Previously, logging data from Hole 642E on the Vøring Margin have revealed a characteristic, asymmetric, cyclic variation in physical properties within subaerially emplaced flood basalts (Barton et al., 1989; Planke, 1994; Delius et al., in press). The average velocity in Hole 642E is about 4 km/s, but the compressional-wave velocity varies from as low as 2.5 km/s in the flow top to as high as 6 km/s in the central and lower part of 5- to 10-m-thick basaltic lavas. Further, the suite of porosity dependent logs (velocity, density, resistivity, and neutron-neutron) generally correlate well (Planke, 1994). Hole 917A provides a possibility to study the physical property variations in lava flows in similar setting, including lavas with different geochemistry and petrology, and thereby better constrain the cause and significance of the characteristic flood basalt log anomalies.

Wireline logs were recorded in about half of the 779-m-thick volcanic sequence in Hole 917A, giving in situ measurements of velocity, density, resistivity, and natural radioactivity. Additionally, the Formation MicroScanner (FMS) was recorded in the hole, giving a detailed borehole wall resistivity image (Demant et al., 1995; Cambray, this volume). The entire suite of logging data has been analyzed in this study, with focuses on (1) evaluating the seismic characteristics of the flood basalt sequence by processing and inversion of sonic waveform data, and (2) conducting detailed log-core correlation, enabled by high core-recovery and high-quality FMS images.

STRATIGRAPHY OF HOLE 917A

Hole 917A was drilled to 875 meters below seafloor (mbsf) with a core recovery of 52% (Figs. 1, 2; Larsen, Saunders, Clift, et al., 1994; Larsen et al., this volume). Two wireline logging runs were re-

¹Saunders, A.D., Larsen, H.C., and Wise, S.W., Jr. (Eds.), 1998. *Proc. ODP, Sci. Results, 152*: College Station, TX (Ocean Drilling Program).

²Department of Geology, University of Oslo, Box 1047 Blindern, 0316 Oslo, Norway. planke@geology.uio.no

³Laboratoire de Mesures en Forage, Institut Méditerranéen de Technologie, 13451 Marseille Cedex 20, France.

corded in the hole: (1) the Formation MicroScanner (FMS) combination (recorded from 595 to 165 mbsf), and (2) the seismic stratigraphy combination (or quad-combo, recorded from 573 to 181 mbsf).

The upper 42 mbsf of Hole 917A consists of glacial and volcanoclastic sediments, followed by 779 m of Paleocene, subaerially emplaced lavas, below which are 54 m of steeply dipping metamorphic claystone and siltstone of possible Paleocene age. The lava stratigraphy was established by Shipboard Scientific Party (1994) with later refinements by Demant et al. (1995). The lavas are divided into three series: a Lower Series of basalts and olivine basalts (821–377 mbsf), a Middle Series of evolved basalts and dacites (377–183 mbsf), and an Upper Series of olivine basalts and picrites (183–42 mbsf). The Lower Series consists predominantly of interlayered thin pahoehoe and thick aa lavas, including two very thin soil layers near the top of

the series (Shipboard Scientific Party, 1994). The lava thickness vary from 1 to 44 m, with an average of 12.5 m. The Middle Series lavas are mostly aa flows, with scoracious, brecciated flow tops and central flow-banding. The flow thickness range is 2 to 53 m (Demant et al., 1995), although the typical thickness is about 6 m. One thin dike intrusion, Unit 39, was identified, while no sediments were found. One 0.6-m-thick sediment layer separates the Middle and Upper Series. The Upper Series consists dominantly of thin pahoehoe lavas with reddened flow tops, including a few thin sediment horizons. The Lower and Middle Series have been dated to around 61 Ma using the ⁴⁰Ar/³⁹Ar method (Sinton et al., 1994; Sinton and Duncan, this volume), while the Upper Series is of uncertain age but not younger than magnetic Chron C24r (ca. 55 Ma). The dip of the lava pile varies with depth, but is roughly 25°SE (Cambray, this volume).

Figure 1. Early Tertiary igneous units and main structural elements in the northeast Atlantic (Eldholm and Grue, 1994). Selected deep drill sites with high core recovery and wireline logs recorded in basalt sequences shown. FDD = Faeroes Deep Drilling Project; IRDP = Iceland Research Drilling Project; OS = Orkustofnun Hole 4, Sugandafjordi. VM = Vøring Margin; HB = Hatton Bank; JL = Jameson Land.

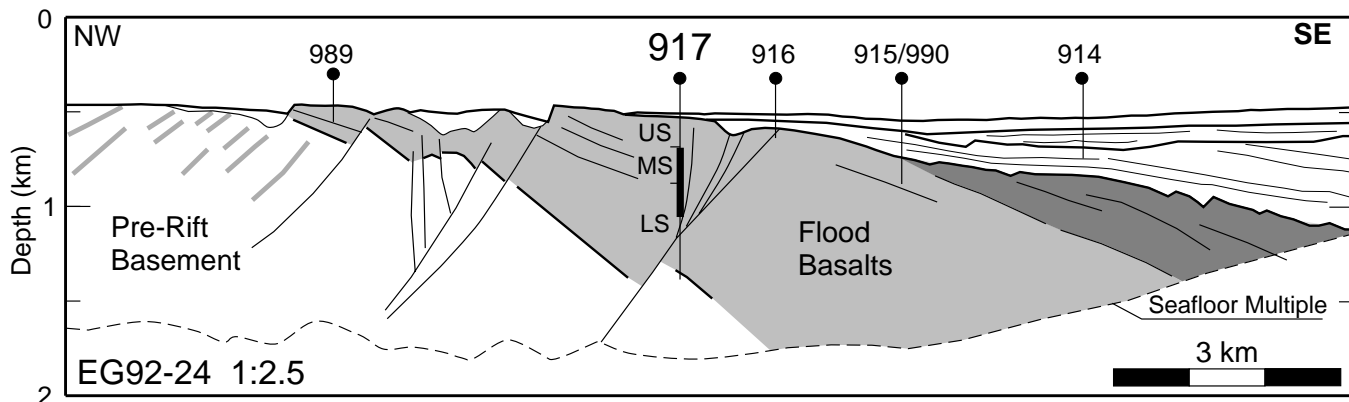
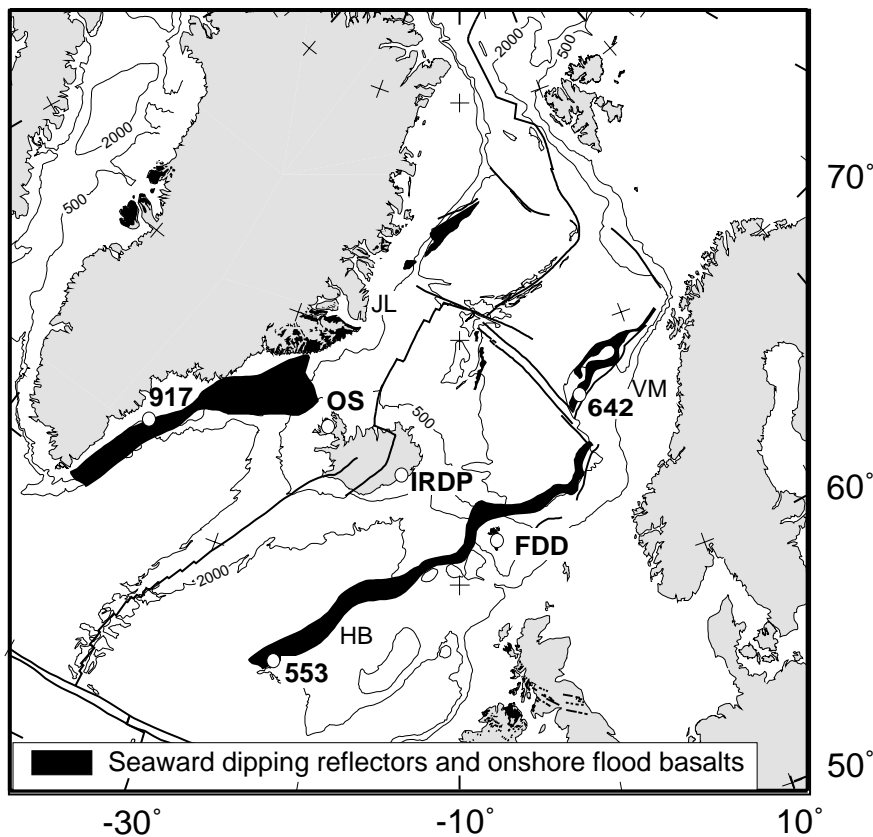


Figure 2. Depth-converted line drawing of the inner part of the EG63 transect on the southeast Greenland Margin with Leg 152 and 163 drill sites located (Duncan, Larsen, Allan, et al., 1996). Bold line shows logged interval. US = Upper Series; MS = Middle Series; LS = Lower Series.

Four logging units have been identified in the hole, corresponding to overall changes in the lava stratigraphy within the Middle and Lower Series (Fig. 3, back pocket; Shipboard Scientific Party, 1994). Logging Unit 1 (181–260 mbsf) is characterized by intermediate natural gamma-ray, velocity, and density values; Unit 2 (260–320 mbsf) by low natural gamma-ray, and high velocity and density values; Unit 3 (320–380 mbsf) primarily by high natural gamma-ray values; and Unit 4 (380–573 mbsf) is characterized by low natural gamma-ray and highly variable velocity and density values.

PROCESSING OF DOWNHOLE DATA

Initial shore-based processing of the wireline logs recorded in Hole 917A include depth shift, as determined by the natural gamma-ray log recorded in both runs, FMS image processing; corrections for borehole size and fluid; and partial elimination of sonic log cycle skips (Shipboard Scientific Party, 1994). The volcano-stratigraphy, coring summary, and various logs recorded in the hole from 185 to 550 mbsf are shown in Figure 3 (back pocket). The digital logging data are included on CD-ROM in the Leg 152 *Initial Reports* volume (Larsen, Saunders, Clift, et al., 1994). The logging tools used by ODP were primarily designed for use in sedimentary basins, but they normally work well in basalt sequences without special processing. For general background regarding the tool measurements and resolution in basalt terrains, see Broglia and Moos (1988), Planke (1994), or Shipboard Scientific Party (1994).

Sonic Digital Tool (SDT) Processing

Compressional-, shear-, and tube-wave velocities and waveform energy logs were determined from processing of the sonic digital tool (SDT) data (Fig. 3, back pocket). The SDT records full waveform data at eight piezo-electric (ceramic) receivers using a sampling frequency of 100 kHz (Harrison et al., 1990). In addition, real-time transit time measurements are obtained using an automatic threshold-based picking routine, and a borehole-compensated sonic log with a vertical resolution of about 0.6 m is subsequently calculated. The noise level during recording of the sonic log was generally high, part-

ly as a result of poor centralization of the tool (Shipboard Scientific Party, 1994). Inspection of the waveform data shows that noisy intervals are commonly associated with unit boundaries, possibly as a result of ringing generated by the previous shot. Noisy data may cause cycle skips which can partially be compensated for by processing of the individual transit time measurements (Shipboard Scientific Party, 1994). This processing, however, was not very successful for the Hole 917A data (Shipboard Scientific Party, 1994).

We have processed the waveform data using a slowness-time coherency method (e.g., Block et al., 1991; Paillet, 1991), where slowness is defined as inverse velocity. The method is based on a modified slant-stack or Radon transform approach (Fig. 4), and is more robust than threshold-based methods (Harrison et al., 1990). The waveform data are initially sorted in a receiver configuration, with the eight microseismograms forming an array with a reference depth in the middle (a common shot point configuration). In the transmitter configuration the microseismograms are re-sorted such that data recorded at a fixed depth point by eight different shots are grouped together, forming a transmitter array (a common receiver configuration) with a vertical resolution of 1 m. The two data sets were processed separately using the slowness-time coherency method (Fig. 4; Table 1), and subsequently averaged and depth-shifted to obtain the final borehole-compensated velocity logs (Fig. 3, back pocket). Tube-waves (or Stoneley-waves) are true boundary waves generated in boreholes (Cheng and Toksöz, 1981). Tube-wave slowness values were obtained in a similar manner as the compressional- and shear-wave slowness values after pre-processing the waveform data with a 1–3-kHz bandpass frequency filter.

Waveform energy logs were calculated from 1–30-kHz and 1–3-kHz filtered microseismograms recorded at the first receiver by summing the squares of amplitudes in a half-cosine tapered time-window as described by Paillet (1991). The logs were subsequently normalized by dividing it with the average of the 100 highest energy values (Fig. 3, back pocket). For shear-waves, the energy was calculated in a 0.6-ms time window using a baseline derived from a 15-point smoothed compressional-wave transit time log and a V_p/V_s ratio of 1.9. The microseismograms were muted after 2 ms to avoid incorporation of fluid- and tube-wave energy, arriving at about 2.05 ms. A minimum window length of 0.2 ms was enforced, and the data were scaled ac-

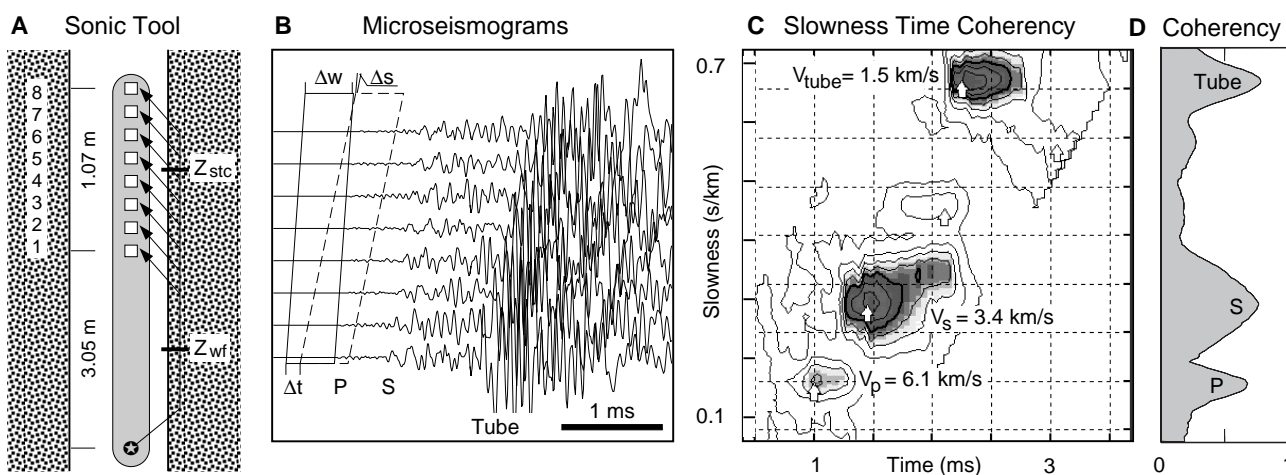


Figure 4. Schematic representation of slowness-time coherency processing. **A.** The sonic signal is recorded at eight receivers. Data are downloaded, quality-controlled, and preprocessed. **B.** The microseismograms for each shot are processed by a modified slant-stack method. The waveform coherency is calculated within a window of width Δw . The slope of the window is then changed by a slowness Δs , and the coherency calculation is repeated. After the coherency is calculated for N slowness values, the window is moved down by a time increment Δt , and the procedure is repeated. **C.** The calculated coherency values are contoured, and peaks in the spectra are automatically determined. **D.** The coherency spectra are projected onto the slowness axis. The final stage involves interactive editing and labeling of coherency peaks in the slowness-projection domain. Z_{stc} = depth-reference for STC processed velocity logs; Z_{wf} = depth-reference for waveform data. P = compressional-wave; S = shear-wave; Tube = tube-wave; V = velocity.

Table 1. Slowness-time coherency processing parameters.

Wave type	Δs ($\mu\text{s}/\text{m}$)	s ($\mu\text{s}/\text{m}$)	Δt (μs)	t (μs)	Δw (μs)	Waveform preprocessing
Compressional (P) and shear (S)	6.5	65–720	50	400–3660	500	Normalization, DC baseline removal
Tube	82	590–1475	200	600–5000	1500	1–3 kHz filter, normalization

Note: See Figure 4 for symbol explanation.

ording to the number of samples in the applied window. A similar approach was used to calculate the tube-wave energy log. The window size was in this case increased to 1.2 ms, no tail mute was applied, and the previously calculated baseline was shifted by 0.7 ms. Fixed sized windows were also tested, but no significant changes in the waveform energy logs were observed. The waveform data are plotted at the midpoint between the transmitter and receiver as the amplitudes are affected by the entire travel path, not only by the differential moveout over the receiver or transmitter array, which is the case for the calculated velocities (Fig. 4).

Other Data

The FMS tool samples about 18% of the borehole wall. The plotted FMS image was horizontally compressed by 80% by deleting most white pixels between the four pads (Fig. 3, back pocket). The relative direction of pad number one is maintained, although the image gives no information about true azimuth or dip. The FMS counts log was constructed by averaging active pixel values along scan lines at each depth level. Because the available FMS data were previously image processed and re-scaled to one-byte numbers (256 levels) the FMS counts log is not directly related to any formation property. The log does, however, give a good indication of the relative changes in borehole wall resistivity.

Minicore velocity and density measurements (Shipboard Scientific Party, 1994) are plotted with the corresponding downhole logs (Fig. 3, back pocket). The data have been relocated to the logging depth scale using the FMS image as a guide wherever possible.

INTERPRETATION OF LOG DATA

Variations Within Single Lava Flows

Log data in Hole 917A, in general, show a cyclic, asymmetric response within each lava flow (Fig. 3, back pocket). Unit 60, an 11.8-m-thick olivine-plagioclase-pyroxene-phyric basalt with 70% recovery, is chosen to illustrate the detailed relations between downhole logs and cores (Fig. 5), as this unit reveals both distinct and typical anomalies and further has no large caliper variations. The lower boundary of Unit 60 was recovered, being defined by the top of a thin lateritic soil with load cast structures. Location of the upper boundary is more uncertain. The log data suggest that a 2.6-m-thick flow, Unit 59, is located between 389.2 and 392.8 mbsf, based on the presence of a 0.5-m-thick high FMS-resistivity interval at 392 mbsf interpreted as representing the interior of a thin flow (Fig. 5). This high-resistivity unit can be correlated with high-velocity anomalies, but may be of limited lateral continuity as it is not well-defined on the deeper resistivity logs. The log-based interpretation as shown on Figure 5 will be used here. In the core, Unit 59 has sharp contact with the overlying plagioclase-olivine-phyric basalt (Unit 58), but no obvious contact with the underlying Unit 60. Finally, note that the logging depth is about 3 m shallower than the drilling depth at the base of Unit 60.

Main Characteristics

The logs recorded in Unit 60 correlate well (Fig. 5). Most log values are low in the upper 3 m, whereas large values are found in the lower 5 to 8 m. The natural gamma-ray log is an exception, being high in the upper part and low in the middle and lower parts. The 1.2-

m-thick high resistivity interval near 397 mbsf (light gray on the FMS image) correlate to distinct anomalies on most logs, in particular high velocities, high resistivities, and low natural gamma-ray values. The fractured interval between 398 and 402 mbsf is clearly identified as a region with lower velocities and resistivities and higher natural gamma ray. The density log shows a slightly different trend, having local maxima both at 397 and 399 mbsf. A probable explanation for the high-density anomaly in a fairly low-velocity and low-resistivity interval is that the density is primarily influenced by total porosity changes while velocity and resistivity are more sensitive to variations in fracture density (e.g., Wilkens et al., 1991; Planke, 1994). The shear-wave velocity log follows, in general, the same trend as the compressional-wave velocity log, while the V_p/V_s ratio varies from 1.7 to 2.2. There is a broad positive correlation between resistivity and the V_p/V_s ratio in the central part of the unit (Fig. 5), but it is not well constrained. The tube-wave travels with a nearly constant velocity of about 0.9 times the borehole fluid velocity in formations where the shear-wave velocity is higher than the fluid velocity (Cheng and Toksöz, 1981) as in the interval from 395 to 402 mbsf. The tube-wave velocity log follows a similar trend as the compressional-wave velocity log in slow formations (e.g., from 390 to 394 mbsf).

The sonic waveform data (Fig. 5) show significant variation in amplitude within Unit 60. The shear-wave energy log has very high values near the unit base. Paillet (1991) found similar very high mode-converted shear-wave amplitudes near fractured intervals in crystalline rocks. These high amplitudes are probably related to mode-conversions across high-impedance boundaries separating low-velocity, vesicular, intervals from high-velocity, massive, formations. The tube-wave energy log follows a similar trend, showing a broad inverse relationship with velocity, and high values near the lower boundary.

Lava Base (402–403.5 mbsf)

The boundary between Unit 60 and an underlying lateritic soil is perfectly recovered in the core, including a nicely developed 2-cm-high load cast structure. The soil is overlain by a highly vesicular flow base and a dense flow interior (see Shipboard Scientific Party, 1994, p. 132). A similar looking structure can be recognized on the FMS image at 403.5 mbsf (Fig. 5), and the lateritic soil is interpreted to be the low resistivity interval just below 403.5 mbsf. Just above the soil is a 10- to 50-cm-thick intermediate resistive zone, corresponding to the vesicular flow base. A 1-m-thick high-resistivity interval overlies the vesicular flow base, continuing upward into the more fractured lava interior. This log-core correlation clearly shows the potential of the FMS log to image internal lava flow structure. However, an even more detailed interpretation can be obtained. A low resistivity structure resembling the load cast structure recovered in the core can be identified on the FMS image at 403.5 mbsf (Fig. 5). The FMS imaged feature is three times bigger (3 by 6 cm) than the recovered load cast structure, but a larger FMS cross section is expected because of the tool resolution limits (Bourke, 1989; Lüthi and Souhaité, 1990). Lateral variations in size of the load cast structure over the 10-cm interval from the drilled core center to the imaged borehole wall is also likely.

The porosity-dependent logs showed large negative gradients in the transition zone from the lava to the underlying soil horizon (402–404 mbsf; Fig. 5). Although resistivity, velocity, and density logs were recorded during the same run, the correlation between the vari-

Table 2. Average compressional-wave velocities, densities, and lava thicknesses measured in Hole 917A.

Depth (mbsf)	V1 (km/s)	V2 (km/s)	V _{p-stc} (km/s)	ρ (g/cm ³)	V _{tube} (km/s)	Z _{ave} (m)
185–550	4.02	4.00	4.17	2.50	1.21	8.7
LU1 (180–260)	3.43	3.40	3.52	2.30	1.13	5.0
LU2 (260–320)	4.56	4.58	4.80	2.70	1.18	15.0
LU3 (320–380)	3.62	3.62	3.79	2.30	1.15	7.1
LU4 (380–550)	4.32	4.31	4.49	2.61	1.28	11.1

Notes: V1 = short-spacing transit-time log velocity, V2 = long-spacing transit-time log velocity, V_{p-stc} = velocity from slowness time coherency processing, ρ = density, V_{tube} = tube-wave velocity, Z_{ave} = average lava thickness, LU = logging unit.

ularity, and fracture density, in addition to fundamental differences in the measurement methods. Hole 917A data show that wireline logs provide an excellent opportunity to define the lava stratigraphy and study internal lava flow structure in holes with no or incomplete recovery.

Large Scale Variations

Compressional-Wave Velocity (V_p)

The sonic velocities in Hole 917A show asymmetric, cyclic variations, with compressional-wave velocity gently increasing from about 3 km/s in the lava top to 5–6 km/s in the central part 5 to 7 m below, before it rapidly decreases near the flow base (Fig. 3, back pocket). The velocity gradient in the upper part of the lavas is fairly constant. The seismic velocities measured on minicore samples correspond poorly with the velocity logs as they are generally too high (Fig. 3, back pocket). The higher velocities measured on the cores are related to preferential sampling of low-porosity, dense intervals both during drilling and minicore sampling.

Average compressional-wave velocities in the lava pile are shown in Table 2. The average slowness-time coherency processed velocity for the logged sequence is 4.17 km/s, 4% higher than the short and long offset sonic log averages. The average basalt sequence velocity based on surface seismic data can be calculated by interpreting the reflector at 1.1 s on profile EG92-24 as the basal unconformity penetrated by Hole 917A at 821 mbsf (Fig. 2). This calculation gives an average velocity of 4.05 km/s, which is very close to the average sonic log velocity. The average sonic velocities of the four logging units varies more, from 3.5 to 4.8 km/s (Table 2). The variations in average velocity between the logging units is primarily related to different lava thickness; the low-velocity logging Unit 1 has a mean unit thickness of 5 m, while the high-velocity logging Unit 2 has a mean unit thickness of 15 m, including the 53-m-thick Unit 52. The average velocity in the lava pile is thus a function of unit thickness as thick flows have a larger proportion of dense, high-velocity material.

V_p/V_s

The receiver and transmitter mode slowness projection coherency plots show high values in the central, dense part of the lavas for both compressional- and shear-waves (Fig. 3, back pocket). The coherency drops significantly in the low-velocity intervals and near flow boundaries resulting in less accurate velocity measurements. Further, note that no shear-waves are generated by the SDT tool in slow formations (i.e., when $V_s < 1.5$ km/s). The receiver mode array generally gives higher coherency values than the transmitter mode array at a given depth (Fig. 3, back pocket) most likely because the waveforms may change between individual shots in the latter case due to varying near-source conditions caused by, for example, changes in lithology or tool centralization.

The shear-wave velocity log generally follows the compressional-wave velocity trend, although large parts of the interval above 360 mbsf have shear-wave velocities below the seawater velocity and could thus not be measured. Cross-plots of V_p and V_s show a good linear correlation, with no large changes from the low- to the high-velocity intervals within individual lavas (Fig. 6). There is a broad bi-

modal distribution in the cross-plots corresponding to the lava flow-top population, having velocities of $V_p \sim 3.8$ km/s and $V_s \sim 2.0$ km/s, and the lava flow-interior population, having velocities of $V_p \sim 5.5$ km/s and $V_s \sim 3.0$ km/s. However, the V_p/V_s ratio is constantly high, typically between 1.8 and 2.0 (Fig. 6).

The fairly constant V_p/V_s ratio within a flow unit is surprising as the data encompass both fairly altered vesicular flow tops and the massive, fractured flow interior. Changes in the V_p/V_s ratio can normally be related to changes in lithology or porosity. Core measurements on fairly unaltered basalts show high V_p/V_s ratios, typically 1.85–1.9 (e.g., Hyndman, 1979; Christensen and Wilkens, 1982; Wilkens et al., 1991). The main alteration products in the Hole 917A lavas are various clay minerals, primarily smectite (Demant, Holmes; both this volume). Shales have high V_p/V_s ratios, commonly in the range from 1.9 to 2.3 (Jones and Wang, 1981; Sayers, 1994). The abundance of clay minerals in the flow tops may suggest an increase in the V_p/V_s ratio from the flow interior to its top. A slight increase in the V_p/V_s ratio with decreasing V_p is apparent in Figure 6, but better low-velocity V_s data are required to confirm this trend.

Waveform Data

The sonic waveform data show large amplitude variations within the logged interval (Fig. 3, back pocket). The shear-wave energy log shows high values near most lava boundaries and within the upper part of a number of basalts. The tube-wave energy log is less spiky, but has local amplitude maxima near unit boundaries between 180 and 360 mbsf. Low values are found in the central part of thick flows, the most notable in the lower 25 m of Unit 52. This is an interval with high velocity but also fractures with slickensides developed on clay surfaces (Shipboard Scientific Party, 1994).

Other Logs

The resistivity and density logs follow, with a few exceptions, the same trend as the velocity logs (Fig. 3, back pocket). The compressional-wave velocity-density cross-plot (Fig. 7A) shows a non-linear trend, with two main populations corresponding to (1) the top, and (2) the central to lower part of individual lavas. Logging Unit 3 is dominated by dacites and shows a quite different cross-plot trend, having a steeper density-velocity relation (Fig. 7B). The spherically focused resistivity and compressional-wave velocity logs show good logarithmic correlation, except in thin high-resistivity units near a few lava bases (Fig. 7C). Similar high resistivity peaks near flow bases are common in Hole 642E (Planke, 1994). In both Holes 642E and 917A the resistivity peaks are typically found above interflow sediments (e.g., Fig. 5). These high-resistivity intervals are possibly related to fast cooling of the base of the lava as it flows across a smoothly undulating soil horizon. A rougher surface is likely to exist when no or only very thin soils are developed. This may result in a more intensely fractured lava base within the overlying flow unit and reduce the development of a high-resistivity zone.

The natural gamma-ray log shows large variations (5–70 GAPI), primarily reflecting variable potassium content in the lava units (Fig. 3, back pocket). Typically, the basalts in logging Units 1 and 2 have values varying between 15 and 30 GAPI. The dacites in logging Unit

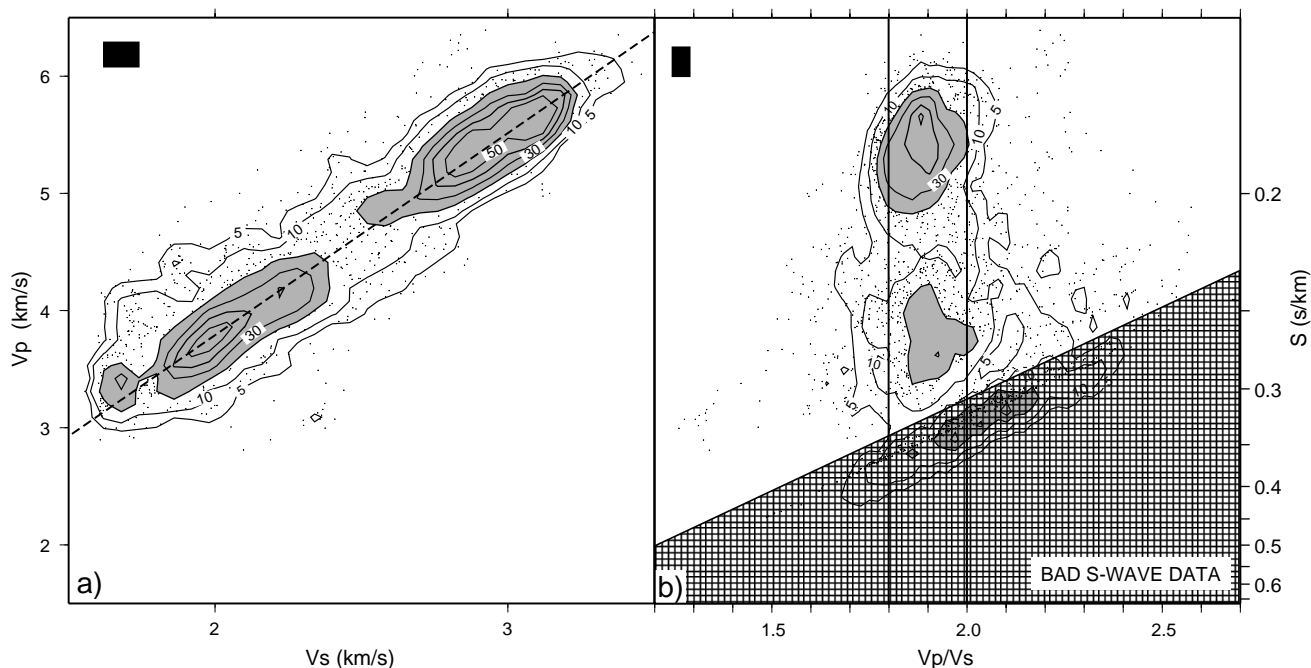


Figure 6. Compressional- and shear-wave velocity crossplots for logging Units 1, 2, and 4, showing fairly constant V_p/V_s ratios. Note that shear-wave velocities are not recorded in slow formations ($V_s < 1.5$ km/s). The logs are smoothed with a seven-point running average (~ 1 m), and the number of points in 50% overlapping rectangles (size in black) contoured. S = slowness.

3 show very high natural gamma-ray values, up to 80 GAPI. The underlying basalts are characterized by low natural radioactivity with exception of high values in Units 70B and 72. Occasionally, there are increased natural gamma ray in the lava tops, while few flows show increasing values with depth (e.g., Units 52 and 67).

DISCUSSION

The comprehensive suite of logging data and high core recovery obtained from ODP Holes 642E and 917A make them suitable reference sites for interpretation of log data from flood basalts. The logged intervals in the holes exhibit a number of morphological and petrological differences. The logs in Hole 642E record a sequence of thin, 2–15 m, tholeiitic basalts, commonly separated by soil horizons (Planke, 1994). Logs in Hole 917A, on the other hand, record dacites, basalts, and picrites with one 53-m-thick unit, and with the presence of only a couple of thin soil layers (Fig. 3, back pocket). Despite such differences the measured physical properties in the two holes are surprisingly similar.

The FMS images in Hole 917A provide a detailed view of the downhole volcano-stratigraphy, and support the interpretation of conventional logs in terms of textural and lithologic variations within flood basalts (Fig. 5). In particular, the flow boundaries are well-defined by the deflection point of the spherically focused resistivity and density logs, but also by the velocity logs, with a vertical resolution of 0.3 to 0.6 m in the absence of large structural dip. The porosity-dependent logs have a bimodal distribution corresponding to (1) a low-porosity, partly fractured flow interior, and (2) an intermediate-to-high-porosity, vesicular, altered interval dominated by the flow top but possibly also including thin interflow sediments and the brecciated base of the overlying lava. The dense interior zone shows relatively small variations in physical properties (e.g., compressional-wave velocity varies between 5 and 6 km/s). The thickness of this zone varies a lot; it is large in thick units, but frequently non-existent in thin (< 5 –7 m) units. The upper vesicular and brecciated zone is always present and is normally up to 7 m thick (Planke, 1994). Physical properties vary greatly within this zone (e.g., compressional-wave veloc-

ity fluctuate from 2.5 to more than 5 km/s), although an overall linear gradient from the top to the base of the zone is apparent. The Hole 642E velocity-density regression line shows a remarkable fit with Hole 917A basalt and picrite units data (Fig. 7A). These systematic changes in physical properties are clearly related to the volcanic emplacement processes, and are in good agreement with models for emplacement of subaerial flood basalts erupted at high rates, forming lavas with dense interiors and brecciated and vesicular flow tops (e.g., Walker, 1993).

On a detailed scale the observed intra-flow velocity changes primarily depend on variations in: (1) clay proportion, (2) total porosity, and (3) pore aspect-ratio distribution. Core and field data from flood basalt terrains (e.g., Shipboard Scientific Party, 1987; Shipboard Scientific Party, 1994) show that all three parameters vary systematically within single lava units. The clay proportion changes from near 100% to 0% from the flow top to its interior. This lithologic change is recorded by the logs, as the estimated matrix velocity and density for shale is about 5.3 km/s and 2.7 g/cm³, respectively (Wyllie et al., 1956), being much lower than typical basalt matrix velocity and density values of 7.0 km/s and 3.0 g/cm³ (Wilkins et al., 1991). The porosity in the upper part of the lavas is dominated by low aspect-ratio vesicles, while the low-porosity interior has a high proportion of high aspect-ratio cracks (Planke, 1994). Rock physics theories have previously been used to estimate changes in total porosity and pore geometries in oceanic basalts based on downhole velocity and density measurements (e.g., Berge et al., 1992). This approach is considered problematic in subaerially emplaced flood basalt sequences as it is difficult to distinguish if velocity and density fluctuations are related to porosity or lithology variations.

The tube-wave energy log in Hole 917A shows lowest values in high-velocity regions in the central part of thick units, in particular within logging Unit 4 (Fig. 3, back pocket), while high tube-wave amplitudes dominate in intervals where the shear-wave velocity is less than the fluid velocity. Attenuation of the sonic waveforms are strongly affected by the presence of fractures or joints in crystalline rocks (e.g., King et al., 1986). The tube-wave energy log can be used quantitatively to estimate fracture permeability and open fractures, as the slow tube-waves are strongly affected by a high attenuation coef-

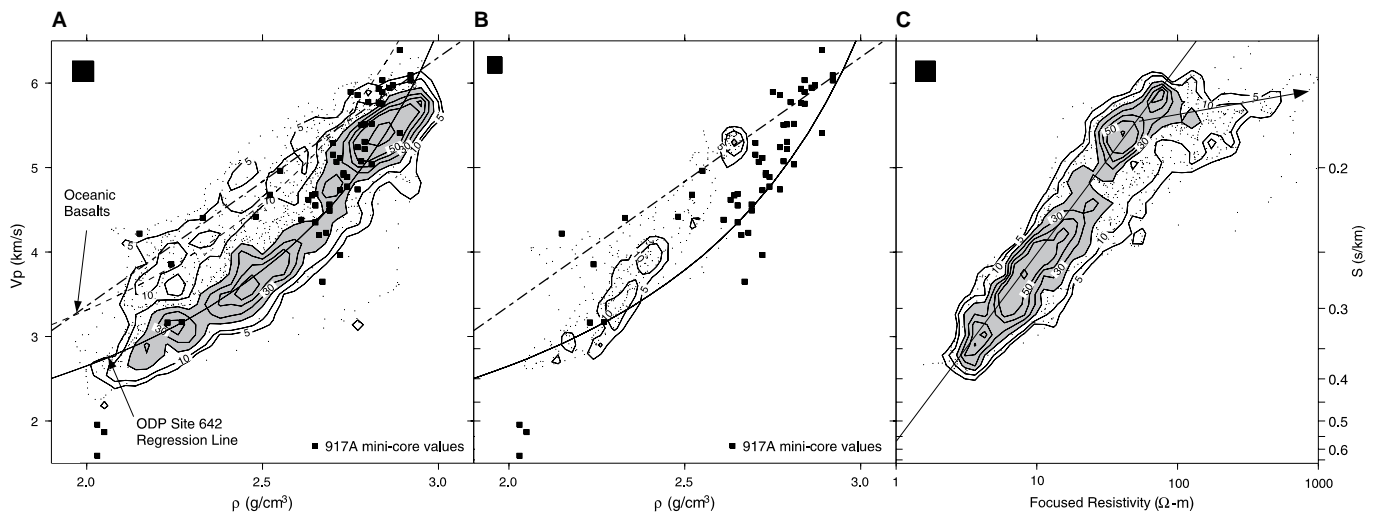


Figure 7. Crossplots of porosity dependent logs. **A.** Velocity-density crossplot in logging Units 1, 2, and 4. Short-dashed line = laboratory measurements of ophiolite and upper oceanic crustal samples (Carlson and Raskin, 1984); bold dashed line = Hole 418A log values (Broglia and Moos, 1988). **B.** Logging Unit 3 (dacites and tuffs) velocity-density crossplot. **C.** Spherically focused resistivity-velocity crossplot, showing a linear trend except for very high-resistivity intervals near the flow bases (arrow).

ficient, Q (Cheng and Toksöz, 1981; Paillet, 1991). The low tube-wave energy in the central part of the thick lavas suggest high attenuation and more open fractures in this zone compared to the altered flow top where cracks are mostly filled with alteration minerals.

The logged Hole 917A lavas (i.e., Lower and Middle Series) were erupted pre-breakup and exhibit a large compositional variation, ranging from picrites through basalts to dacites (Shipboard Scientific Party, 1994). The lavas exhibit a large thickness range, from 1 to 53 m. The natural gamma-ray log show distinct variations between the various logging units, being dominantly low (5–10 GAPI) in basalts in logging Unit 4 and high (25–75 GAPI) in the dacites in logging Unit 3 (Fig. 3, back pocket). High natural gamma-ray peaks (15–30 GAPI) are frequently recorded between lava units in Hole 642E, and are interpreted as altered flow tops and interflow sediments (Planke, 1994). The frequency and thickness of interflow sediments is a qualitative indication of time duration between eruptions (Shipboard Scientific Party, 1987). High natural gamma-ray peaks are generally absent in Hole 917A, with notable exceptions near the top of Units 59–61 and 67 (Fig. 3, back pocket). Sediments 5 cm thick are recovered from the top two of these units (Shipboard Scientific Party, 1994). The general absence of high natural gamma-ray peaks and interflow sediments in Hole 917A suggests fairly rapid construction of the lava pile in a near-source environment, compared with the more distal lavas found in Hole 642E. The natural gamma-ray peaks in units near the top of the Lower Series may correspond to a period with vanishing volcanism leading up to the more vigorous volcanism associated with the Middle Series dacites, tuffs, and the very thick basalt Unit 52. A similar decrease in volcanism is interpreted to occur just before the Lower to Middle Series transition on the Faeroes (Noe-Nygaard and Rasmussen, 1984).

Implications for Seismic Wave Propagation

Strong converted waves are identified on wide-angle seismic data in flood basalt terrains, giving high V_p/V_s ratios of 1.8–1.9 in the basalt sequences (Barton et al., 1989; Myhre et al., 1995; Flóvenz and Gunnarsson, 1991). Similar high V_p/V_s ratios of 1.8–2.0 is found from SDT processed velocity data in Hole 917A. The high-amplitude converted waves are commonly interpreted as mode-conversions from high-impedance boundaries separating sediments and the underlying basalt sequence. The Hole 917A sonic waveform data show,

however, that strong converted waves also can be generated within the lava pile due to high impedance boundaries between the lavas and within the upper part of individual flows. The possibility of mode-converted waves generated within the lava pile is further corroborated by observation of strong shear-waves in purely basalt terranes (e.g., on refraction data from Iceland; Flóvenz and Gunnarsson, 1991).

Large flow-scale variations in seismic properties in subaerially emplaced flood basalts are confirmed by the Hole 917A logging data. Propagation of long period (10–60 Hz) waves in flood basalt sequences is therefore obviously poorly described by a homogenous, isotropic earth model. Intra-basement basalt reflectors are dominantly interference phenomenon, although thick flows may generate distinct reflectors (Planke and Eldholm, 1994). The systematic layering of high- and low-velocity intervals within the subaerially emplaced basalt sequence suggests that the sequence is anisotropic, with at least a hexagonal symmetry (transverse isotropy). The anisotropy was estimated to be 10% to 20% from wave equation modeling and comparison of vertical seismic profile (VSP) experiments and wide-angle surveys on the Vøring Plateau and in the Tertiary flood basalts in Iceland (Planke and Eldholm, 1994; Planke and Flóvenz, 1994, 1996). More general equivalent-media representation accounting for both transmissivity and reflectivity (e.g., Shapiro et al., 1996) may be difficult to obtain in these areas as the local velocity fluctuations are large.

At Sites 642 and 917 the average vertical velocity is estimated from VSP and MCS data, respectively, and are in both cases very similar to the average compressional-wave sonic log velocity. In Hole 917A the average sonic basalt velocities are between 4.0 and 4.2 km/s while the average MCS-calculated velocity is 4.05 km/s (Table 2). Similarly, in Hole 642E the average sonic velocity is 3.9 km/s while the VSP derived velocity is 3.8 km/s (Planke and Eldholm, 1994). Variations in average lava flow thickness is the main factor determining regional variations in the near-vertical velocity structure in subaerially emplaced basalt sequences (Fig. 8). Large changes in average unit thickness is observed on the Faeroes where the average thickness of the lavas drilled by the Lopra-1 hole is 20 m, significantly higher than the average thickness of 2.2 m in the stratigraphically overlying sequence penetrated by the Vestmanna-1 hole (Waagstein and Hald, 1984). Downhole logs recorded to about 2.1-km-depth in Lopra-1 show a cyclic log pattern (Nielsen et al., 1984; Stefánsson

and Tulinius, 1983), not unlike Holes 917A and 642E data. The recorded sonic log was unfortunately of poor quality, though a mean of 4.35 ± 0.32 km/s and a maximum of 4.55 km/s was found (Nielsen et al., 1984). The suite of log data suggest similar seismic properties as found in Holes 917A and 642E. Thus, the expected average velocity of Lopra-1 is 4.8 km/s while the expected average velocity of Vestmanna-1 is 3.3 km/s (Fig. 8). A zero-offset VSP experiment in Lopra-1 gives interval velocities of 4.8–6.2 km/s, with an average of about 5.5 km/s in the lower 1.5 km (Kjørboe and Petersen, 1995). However, two thick dikes were penetrated by Lopra-1 (Nielsen et al., 1984), and a northwest-trending near-vertical dike is outcropping just east of Lopra-1 (Rasmussen and Noe-Nygaard, 1990). The discrepancy between the expected average velocity of 4.8 km/s and the observed VSP velocity of 5.5 km/s is tentatively interpreted as due to the dike intrusions acting as high-velocity wave-channels.

CONCLUSIONS

Standard seismic stratigraphy and FMS tool strings were run through a 430-m-thick volcanic interval penetrated by Hole 917A near the landward-edge of the SDRS on the southeast Greenland Margin. The FMS image and recovered core data (52% recovery) show that the conventional porosity-dependent logs (velocity, density, resistivity) confidently can be used to interpret downhole textural and lithologic changes in flood basalt sequences, and that they are well-suited to define the downhole volcano stratigraphy. The log data reveal an asymmetric, cyclic response, related to systematic changes in total porosity, pore aspect-ratio distribution, and clay alteration minerals. The sonic velocity distribution is generally bimodal, with highly variable, downward increasing velocities of 2.5 to 5.5 km/s in the upper 5 to 7 m of the lavas and more uniform velocities of 5 to 6 km/s in the flow interior. The log characteristics are very similar to log data recorded in flood basalt sequences elsewhere, such as Hole 642E on the Vøring Margin, but differ from logs recorded in oceanic basalts. The range of high-quality downhole data obtained in both Holes 917A and 642E suggests that they are well-suited as logging reference sites in flood basalt terranes.

Thin interflow sediments are identified by high natural gamma-ray peaks near the lava top and high spherically focussed resistivity peaks near the base of the overlying lava. Both these features are generally absent in Hole 917A with the exception of lavas in the upper part of the Lower Series. The presence of interflow sediments suggests longer time intervals between lava emplacement leading up to the more explosive, vigorous volcanism recorded as tuffs, dacites, and very thick flows in the Middle Series. In general, the logged Hole 917A lavas are interpreted as being rapidly emplaced.

The full waveform sonic data were processed using a slowness-time coherency method to obtain shear- and tube-wave velocities in addition to an improved compressional-wave velocity log. The calculated V_p/V_s ratio is between 1.8 and 2.0, and no systematic changes within the lava pile are observed. Low-velocity lava flow-tops are severely undersampled, as the shear-waves only were measured in high-velocity intervals ($V_s > 1.5$ km/s). Shear- and tube-wave energy logs reveal high-values near unit boundaries and low values in high-velocity lava interiors. These observations suggest that strong shear-waves observed in flood basalt terrains are partly mode-converted within the lava pile. Minicore velocity and density values relocated to the logging depth scale show poor correlation with the observed logs. This is primarily related to biased minicore sampling of unfractured, dense parts of the lava flows.

The average compressional-wave velocity is 4.17 km/s, very close to the 4.05 km/s calculated from the interpreted MCS data. The average velocity is primarily a function of systematic variations in mean lava flow thickness. The high-impedance contrasts within and between the lava flows give rise to strong reflections and converted

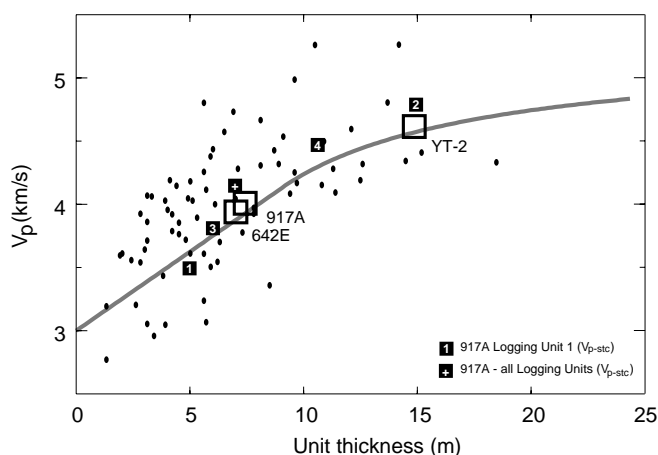


Figure 8. Average compressional-wave velocity vs. lava thickness showing that the basalt thickness is an important parameter for determining the overall velocity structure of flood basalt sequences. Solid curve calculated from the characteristic velocity log distribution for Hole 642E lavas; solid circles are mean velocities in the fine-grained basalts (Planke, 1994). Open squares show average velocities as determined by VSP data (Holes 642E and YT-2) and seismic reflection data (Hole 917A) (Planke and Flóvenz, 1996); solid squares are the average STC-processed velocities in Hole 917A logging units (Table 2).

waves, while reflections are normally interference phenomenon in the absence of very thick lavas (>20 m). The layering of the lava sequence further gives rise to anisotropic wave-propagation, being faster in the horizontal than the vertical direction.

ACKNOWLEDGMENTS

We would like to thank GeoQuest (Stavanger) for access to their slowness-time coherency processing software, and the authors of the public domain GMT (Wessel and Smith, 1991) and Seismic Unix software packages. This work was supported by the ProPetro program of the Research Council of Norway and Statoil. Finally, we would like to thank C.J. Bucker, O. Eldholm, G.J. Fryer, and H.C. Larsen for providing constructive reviews and comments.

REFERENCES

- Barton, C., Moos, D., and Blangy, J.-P., 1989. Analysis of full waveform acoustic logging data at ODP Site 642—outer Vøring Plateau. *In* Eldholm, O., Thiede, J., Taylor, E., et al., *Proc. ODP, Sci. Results*, 104: College Station, TX (Ocean Drilling Program), 953–964.
- Berge, P.A., Fryer, G.J., and Wilkens, R.H., 1992. Velocity-porosity relationships in the upper oceanic crust: theoretical considerations. *J. Geophys. Res.*, 97:15239–15254.
- Block, L.V., Cheng, C.H., and Duckworth, G.L., 1991. Velocity analysis of multireceiver full-waveform acoustic-logging data in open and cased holes. *Log Analyst*, 32:188–200.
- Blystad, P., Brekke, H., Færseth, R.B., Larsen, B.T., Skogseid, J., and Tørudbakken, B., 1995. Structural elements of the Norwegian continental shelf, Part II: the Norwegian Sea region. *Norw. Petrol. Direct. Bull.*, 8.
- Boldreel, L.O., and Andersen, M.S., 1994. Tertiary development of the Faeroe-Rockall Plateau based on reflection seismic data. *Bull. Geol. Soc. Den.*, 41:162–180.
- Bourke, L.T., 1989. Recognizing artifact images of the formation microscanner. *SPWLA 30th Ann. Logging Symp.*, paper WW.
- Brogliola, C., and Moos, D., 1988. In-situ structure and properties of 110-Ma crust from geophysical logs in DSDP Hole 418A. *In* Salisbury, M.H., Scott, J.H., et al., *Proc. ODP, Sci. Results*, 102: College Station, TX (Ocean Drilling Program), 29–47.

- Carlson, R.L., and Raskin, G.S., 1984. Density of the ocean crust. *Nature*, 311:555–558.
- Cheng, C.H., and Toksöz, M.N., 1981. Elastic wave propagation in a fluid-filled borehole and synthetic acoustic logs. *Geophysics*, 46:1042–1053.
- Christensen, N.I., and Wilkens, R.H., 1982. Seismic properties, density and composition of the Icelandic crust near Reydarfjörður. *J. Geophys. Res.*, 87:6389–6395.
- Coffin, M.F., and Eldholm, O., 1994. Large igneous provinces: crustal structure, dimensions, and external consequences. *Rev. Geophys.*, 32:1–36.
- Delius, H., Bücker, C., and Wohlenberg, J., in press. Basaltic lava flows and volcanoclastic sediments and their significant log responses. *Sci. Drill.*
- Demant, A., Cambray, H., Vandamme, D., and Leg 152 Shipboard Scientific Party, 1995. Lithostratigraphy of the volcanic sequences at Hole 917A, Leg 152, Southeast Greenland margin. *J. Geol. Soc. London*, 152:943–946.
- Duncan, R., Larsen, H.C., Allan, J., et al., 1996. *Proc. ODP, Init. Repts.*, 163: College Station, TX (Ocean Drilling Program).
- Eldholm, O., and Grue, K., 1994. North Atlantic volcanic margins: dimensions and production rates. *J. Geophys. Res.*, 99:2955–2968.
- Eldholm, O., Skogseid, J., Planke, S., and Gladczenko, T.P., 1995. Volcanic margin concepts. In Banda, E., Talwani, M., and Torne, M. (Eds.), *Rifted Ocean-Continent Boundaries*. NATO ASI Ser. 1–16.
- Eldholm, O., Thiede, J., Taylor, E., et al., 1987. *Proc. ODP, Init. Repts.*, 104: College Station, TX (Ocean Drilling Program).
- Flóvenz, Ó.G., Georgsson, L.S., and Árnason, K., 1985. Resistivity structure of the upper crust in Iceland. *J. Geophys. Res.*, 90:10136–10150.
- Flóvenz, Ó.G., and Gunnarsson, K., 1991. Seismic crustal structure in Iceland and surrounding area. *Tectonophysics*, 189:1–18.
- Harrison, A.R., Randall, C.J., Aron, J.B., Morris, C.F., Wignall, A.H., Dworak, R.A., Rutledge, L.L., and Perkins, J.L., 1990. Acquisition and analysis of sonic waveforms from a borehole monopole and dipole source for the determination of compressional and shear speeds and their relation to rock mechanical properties and surface seismic data. *Abstract 65, Ann. Tech. Conf. Exhib. Soc. Pet. Eng.*, 23–26/9, 267–282.
- Hinz, K., Mutter, J.C., Zehnder, C.M., and NGT Study Group, 1987. Symmetric conjugation of continent-ocean boundary structures along the Norwegian and East Greenland margins. *Mar. Pet. Geol.*, 3:166–187.
- Hyndman, R.D., 1979. Poisson's ratio in the oceanic crust—a review. *Tectonophysics*, 49:321–333.
- Jones, L.E.A., and Wang, H.F., 1981. Ultrasonic velocities in Cretaceous shales from the Williston basin. *Geophysics*, 46:288–297.
- King, M.S., Myer, L.R., Rezowaalli, J.J., 1986. Experimental studies of elastic-wave propagation in a columnar-jointed rock mass. *Geophys. Prospect.*, 34:1185–1199.
- Kjørboe, L., and Petersen, S.A., 1995. Seismic investigation of the Faeroe basalts and their substratum. *Geol. Soc. Spec. Publ. London*, 90:111–122.
- Larsen, H.C., 1990. The East Greenland Shelf. In Grantz, A., Johnson, G.L., and Sweeney, J.F. (Eds.), *The Arctic Ocean Region*. Geol. Soc. Am., Geol. of North Am. Ser., L:185–210.
- Larsen, H.C., Saunders, A.D., Clift, P.D., et al., 1994. *Proc. ODP, Init. Repts.*, 152: College Station, TX (Ocean Drilling Program).
- Lüthi, S.M., and Souhaité, P., 1990. A method for fracture extraction and width determination from electrical borehole scans. *Geophysics*, 55:821–833.
- Myhre, B., Mjelde, R., Sellevoll, M.A., and Kodaira, S., 1995. Shear waves from three-component ocean bottom seismographs off Lofoten, Norway. *EGS 20th Ann. Meeting*, p.127.
- Nielsen, P.H., Stefánsson, V., and Tulinius, H., 1984. Geophysical logs from Lopra-1 and Vestmanna-1. In Berthelsen, O., Noe-Nygaard, A., and Rasmussen, J. (Eds.), *The Deep Drilling Project 1980–1981 in the Faeroe Islands: Tórshavn (Føroya Fróðskaparfelag)*, 115–135.
- Noe-Nygaard, A., and Rasmussen, J., 1984. Introduction: geological review and choice of drilling sites. In Berthelsen, O., Noe-Nygaard, A., and Rasmussen, J. (Eds.), *The Deep Drilling Project 1980–1981 in the Faeroe Islands: Tórshavn (Føroya Fróðskaparfelag)*, 9–12.
- Paillet, F.L., 1991. Qualitative and quantitative interpretation of fracture permeability using acoustic full-waveform logs. *Log Analyst*, 32:256–270.
- Pezard, P.A., and Anderson, R.N., 1989. Morphology and alteration of the upper oceanic crust from in-situ electrical experiments in DSDP/ODP Hole 504B. In Becker, K., Sakai, H., et al., *Proc. ODP, Sci. Results*, 111: College Station, TX (Ocean Drilling Program), 133–146.
- Planke, S., 1994. Geophysical response of flood basalts from analysis of wireline logs: Ocean Drilling Program Site 642, Vøring volcanic margin. *J. Geophys. Res.*, 99:9279–9296.
- Planke, S., and Eldholm, O., 1994. Seismic response and construction of seaward dipping wedges of flood basalts: Vøring volcanic margin. *J. Geophys. Res.*, 99:9263–9278.
- Planke, S., and Flóvenz, O.G., 1994. Integration of downhole and surface seismic data in flood basalt terrains: implications for seismic imaging and crustal structure. *Am. Geophys. Union Fall Meeting*. (Abstract)
- , 1996. Seismic properties of flood basalts. *Norw. Pet. Soc. Conference on Seismic Lithology*. (Abstract)
- Rasmussen, J., and Noe-Nygaard, A., 1990. The origin of the Faeroe Islands (text and maps). *Den. Geol. Surv.*
- Roberts, D.G., Schnitker, D., et al., 1984. *Init. Repts. DSDP*, 81: Washington (U.S. Govt. Printing Office).
- Sayers, C.M., 1994. The elastic anisotropy of shales. *J. Geophys. Res.*, 99:767–774.
- Shapiro, S.A., Hubral, P., and Ursin, B., 1996. Reflectivity/transmissivity for one-dimensional inhomogeneous random elastic media: dynamic-equivalent-medium approach. *Geophys. J. Int.*, 126:184–196.
- Shipboard Scientific Party, 1987. Site 645. In Srivastava, S.P., Arthur, M., Clement, B., et al., *Proc. ODP, Init. Repts.*, 105: College Station, TX (Ocean Drilling Program), 61–418.
- , 1994. Site 917. In Larsen, H.C., Saunders, A.D., Clift, P.D., et al., *Proc. ODP, Init. Repts.*, 152: College Station, TX (Ocean Drilling Program), 107–158.
- Sinton, C.W., Larsen, H.C., and Duncan, R.A., 1994. The timing of the volcanism at the southeast Greenland Margin, ODP Leg 152. *Eos*, 75:607.
- Stefánsson, V., and Tulinius, H., 1983. Geophysical logs from Lopra-1 and Vestmanna-1. *Orkustofnun Rep. OS-83088/JHD-18*, Reykjavik, Iceland.
- Waagstein, R., and Hald, N., 1984. Structure and petrography of a 660 m lava sequence from the Vestmanna-1 drill hole, lower and middle basalt series, Faeroe Islands. In Berthelsen, O., Noe-Nygaard, A., and Rasmussen, J. (Eds.), *The Deep Drilling Project 1980–81 in the Faeroe Islands: Tórshavn (Føroya Fróðskaparfelag)*, 39–70.
- Walker, G.P.L., 1993. Basaltic-volcano systems: magmatic processes and plate tectonics. *Geol. Soc. Spec. Publ. London*, 76:3–38.
- Wessel, P., and Smith, W.H.F., 1991. Free software helps map and display data. *Eos*, 72:441–446.
- White, R.S., Spence, G.D., Fowler, S.R., McKenzie, D.P., Westbrook, G.K., and Bowen, A.N., 1987. Magmatism at rifted continental margins. *Nature*, 330:439–444.
- Wilkens, R.H., Fryer, G.J., and Karsten, J., 1991. Evolution of porosity and seismic structure of upper oceanic crust: importance of aspect ratios. *J. Geophys. Res.*, 96:17891–17995.
- Wyllie, M.R.J., Gregory, A.R., and Gardner, L.W., 1956. Elastic wave velocities in heterogeneous and porous media. *Geophysics*, 21:41–70.
- Zehnder, C.M., Mutter, J.C., and Buhl, P., 1990. Deep seismic and geochemical constraints on the nature of rift-induced magmatism during breakup of the North Atlantic. *Tectonophysics*, 173:545–565.

Date of initial receipt: 4 November 1995

Date of acceptance: 11 November 1996

Ms 152SR-247